The Astrophysical Journal, 673:119–127, 2008 January 20

SPITZER MID-INFRARED SPECTROSCOPY OF 70 μm–SELECTED DISTANT LUMINOUS INFRARED GALAXIES

Kate Brand,[1] Dan W. Weedman,[2] Vandana Desai,[3] Emeric Le Floc'h,[4,5] Lee Armus,[6] Arjun Dey,[7] Jim R. Houck,[2] Buell T. Jannuzi,[7] Howard A. Smith,[8] and B. T. Soifer[3,6]

Received 2007 August 6; accepted 2007 September 17

ABSTRACT

We present mid-infrared spectroscopy obtained with the *Spitzer Space Telescope* of a sample of 11 optically faint, infrared luminous galaxies selected from a *Spitzer* MIPS 70 μm imaging survey of the NDWFS Boötes field. These are the first *Spitzer* IRS spectra presented of distant 70 μm–selected sources. All the galaxies lie at redshifts $0.3 < z < 1.3$ and have very large infrared luminosities of $L_{\rm IR} \sim (0.1\text{–}17) \times 10^{12}\ L_{\odot}$. Seven of the galaxies exhibit strong emission features attributed to polycyclic aromatic hydrocarbons (PAHs). The average IRS spectrum of these sources is characteristic of classical starburst galaxies but with much larger infrared luminosities. The PAH luminosities of $\nu L_{\nu}(7.7\ \mu{\rm m}) \sim (0.4\text{–}7) \times 10^{11}\ L_{\odot}$ imply star formation rates of $\sim$40–720 $M_{\odot}\ {\rm yr}^{-1}$. Four of the galaxies show deep 9.7 μm silicate absorption features and no significant PAH emission features (6.2 μm equivalent widths <0.03 μm). The large infrared luminosities and low $\nu f_{\nu}(70\ \mu{\rm m})/\nu f_{\nu}(24\ \mu{\rm m})$ flux density ratios suggests that these sources have AGNs as the dominant origin of their large mid-infrared luminosities, although deeply embedded but luminous starbursts cannot be ruled out. If the absorbed sources are AGN-dominated, a significant fraction of all far-infrared bright, optically faint sources may be dominated by AGNs.

Subject headings: galaxies: active — galaxies: starburst — infrared: galaxies — quasars: general

Online material: color figures

1. INTRODUCTION

Luminous and ultraluminous infrared galaxies [LIRGs: $L(8\text{–}1000\ \mu{\rm m}) > 10^{11}\ L_{\odot}$; Sanders et al. 1988] have been studied extensively in the local universe with the *Infrared Astronomical Telescope* (*IRAS*; Soifer et al. 1987; Saunders et al. 1990), the *Infrared Space Observatory* (*ISO*; e.g., Lutz et al. 1998; Genzel & Cesarsky 2000; Tran et al. 2001), and more recently, with the Infrared Spectrograph (IRS; Houck et al. 2004) on *Spitzer* (Weedman et al. 2005; Brandl et al. 2006; Armus et al. 2007; Desai et al. 2007). These galaxies exhibit a large range of properties in the mid-IR, some showing strong polycyclic aromatic hydrocarbon (PAH) emission features characteristic of powerful (up to $\approx$1000 $M_{\odot}\ {\rm yr}^{-1}$) star formation rates (e.g., Brandl et al. 2006; Smith et al. 2007), and all exhibiting a large range in 9.7 μm silicate absorption or emission strengths (e.g., Weedman et al. 2005; Desai et al. 2007; Imanishi et al. 2007). *Spitzer* IRS is now enabling the study of the mid-infrared spectra of LIRGs to much higher redshifts ($z \sim 2.6$; Houck et al. 2005 Yan et al. 2005). Although rare locally, LIRGs become an important population at high redshifts and account for an increasing fraction of the star formation activity in the universe (Le Floc'h et al. 2005). By studying their infrared properties, one can estimate the extent to which AGNs and star formation contribute to their infrared luminosities and therefore determine a correct census of starbursts and AGNs at epochs in the universe when their luminosity density was at its maximum.

A particularly interesting population of high-redshift, optically faint infrared sources has been discovered using the Multiband Imaging Photometer for *Spitzer* (MIPS; Rieke et al. 2004). Various observing programs with *Spitzer* IRS have found that MIPS sources at flux density levels of $f_{\nu}(24\ \mu{\rm m}) \sim 1$ mJy with optical magnitudes $R \gtrsim 24$ Vega magnitudes are typically at $z \sim 2$ (Houck et al. 2005; Yan et al. 2007; Weedman et al. 2006b). Most of the sources are characterized by strong absorption by the 9.7 μm silicate feature, but sources chosen with an additional indicator of star formation (submillimeter detection or shape of the spectral energy distribution) often shown strong PAH emission features (Lutz et al. 2005; Weedman et al. 2006a; Menéndez-Delmestre et al. 2007; Yan et al. 2007; Sajina et al. 2007). Using traditional optical techniques to characterize these sources is difficult because they are too faint in the optical band. Mid-infrared spectroscopy is the best currently available tool in understanding these sources, but we need to learn how to categorize them from the different features that are exhibited in the infrared band. We might expect sources that are selected on the basis of their large far-infrared flux densities to contain large amounts of cool dust and show signatures of starbursts. Mid-infrared spectroscopy of these sources will test this assumption and may help our understanding of high-redshift LIRGs as a whole.

In this paper, we present the first *Spitzer* IRS spectra of a small sample of galaxies selected on the basis of their large 70 μm flux densities and optical faintness. We have previously reported results on sources chosen only with criteria of large infrared to optical flux ratios, as measured by comparison of their 24 μm flux density, $f_{\nu}(24\ \mu{\rm m})$ with optical magnitude ($R - [24] > 14$; Houck et al. 2005; Weedman et al. 2006b). We now extend the IRS observations to additional sources in Boötes that are less extreme in their $R-[24]$ colors but are selected with the additional criteria

[1] Space Telescope Science Institute, 3700 San Martin Drive, Baltimore, MD 21218; brand@stsci.edu.
[2] Astronomy Department, Cornell University, Ithica, NY 14853.
[3] Division of Physics, Mathematics and Astronomy, California Institute of Technology, 320-47, Pasadena, CA 91125.
[4] Institute for Astronomy, University of Hawaii, 2680 Woodlawn Drive, Honolulu, HI 96822.
[5] *Spitzer* fellow.
[6] *Spitzer* Science Center, California Institute of Technology, 220-6, Pasadena, CA 91125.
[7] National Optical Astronomy Observatory, 950 North Cherry Avenue, Tucson, AZ 85726.
[8] Harvard-Smithsonian Center for Astrophysics, 60 Garden Street, Cambridge, MA 02138.

TABLE 1
Optical and IR Properties

IRS ID	MIPS Name	B_W[a,b] (mag)	R[a,b] (mag)	I[a,b] (mag)	K[a,b] (mag)	$f_{3.6}$[c] (mJy)	$f_{4.5}$[c] (mJy)	$f_{5.8}$[c] (mJy)	f_8[c] (mJy)	f_{24}[c] (mJy)	f_{70} (mJy)	f_{160} (mJy)	$R-[24]$ (mag)
70Bootes1	SST24 J142651.9+343135	22.7	20.6	19.8	16.7[d]	0.11	0.09	0.08	0.17	1.39	32.8 ± 4.2	<120	11.3
70Bootes2	SST24 J142732.9+324542	22.7	20.7	19.9	...	0.07	0.07	0.09	0.21	1.22	34.6 ± 4.1	<120	11.2
70Bootes3	SST24 J143639.0+345222	23.2	22.0	21.1	...	0.13	0.10	0.10	0.12	1.26	35.0 ± 6.3	145 ± 29	12.6
70Bootes4	SST24 J143218.1+341300	23.3	22.0	21.0	17.8[e]	0.10	0.09	0.09	0.12	1.22	36.6 ± 5.1	100 ± 20	12.6
70Bootes5	SST24 J143050.8+344848	...	24.6	22.4	...	0.04	0.04	0.08	0.24	4.25	43.2 ± 5.1	70 ± 14	16.5
70Bootes6	SST24 J143830.6+344412	23.8	21.1	18.7	...	0.13	0.14	0.22	0.78	3.19	45.2 ± 4.0	<120	12.7
70Bootes7	SST24 J143151.8+324327	22.3	20.5	19.7	...	0.20	0.16	0.17	0.37	2.18	51.8 ± 4.7	135 ± 27	11.7
70Bootes8	SST24 J143341.9+330136	22.7	21.1	20.2	17.8[e]	0.08	0.06	0.09	0.21	4.72	63.2 ± 3.9	105 ± 21	13.1
70Bootes9	SST24 J143820.7+340233	22.7	20.3	19.3	15.7[e]	0.40	0.27	0.32	0.34	3.46	67.2 ± 3.1	245 ± 49	12.0
70Bootes10	SST24 J143449.3+341014	23.6	21.5	20.7	17.5[e]	0.25	0.23	0.68	0.97	2.19	94.5 ± 4.5	120 ± 24	12.7
70Bootes11[f]	SST24 J143205.6+325835	21.3	20.1	19.8	...	0.08	0.13	0.27	1.3	16.66	115.8 ± 12.8	<120	13.5

[a] All quoted magnitudes are Vega magnitudes from the NDWFS DR3 (B. T. Jannuzi et al. 2008, in preparation).
[b] Errors on B_w, R, I, and K-band magnitudes are <0.1.
[c] Errors on $f_{3.6}$, $f_{4.5}$, $f_{5.8}$, f_8, and f_{24} flux densities are <0.1 mJy.
[d] K-mag from NDWFS survey (A. Dey et al. 2008, in preparation).
[e] K_s-mag from FLAMEX survey (Elston et al. 2006).
[f] Object 8 in Houck et al. (2007).

of detection at 70 μm by *Spitzer* MIPS. A cosmology of $H_0 = 70$ km s^{-1} Mpc^{-1}, $\Omega_M = 0.3$, and $\Omega_\Lambda = 0.7$ is assumed throughout.

2. SOURCE SELECTION

We selected a sample of optically faint, far-infrared luminous sources from the *Spitzer* MIPS 70 μm survey of the NOAO Deep Wide-Field (NDWFS; Jannuzi & Dey 1999) Boötes field for follow-up with *Spitzer* IRS. Such sources have not previously been studied, and our paper provides the first census of their basic mid-IR properties. The 70 μm observations reach a 5 σ limiting flux density of $f_{70\,\mu\mathrm{m}} = 25$ mJy and yield a total of $\approx$330 sources. To ensure a highly reliable 70 μm catalog and allow follow-up observations with IRS, we only included 70 μm sources with a 24 μm flux density, $f_{24} > 1$ mJy and $f_{70\,\mu\mathrm{m}} >$ 30 mJy (this resulted in only 16 rejected sources and should not bias our sample to sources with unusually high 24 μm flux densities). We measured optical photometry in the publicly available NDWFS R-band images and selected all sources with $R \geq$ 20 Vega mag. Although ideally we would like to select sources as red in their optical to infrared colors as the $R - [24] > 14$ sources previously observed in the Boötes field, the lack of available candidates has required us to relax this criteria. Our sample has a larger range of optical to infrared colors corresponding to $11 < R - [24] < 16.5$. Although the optical obscuration is likely to be less extreme, the combined faint optical and bright infrared selection should still select distant infrared bright galaxies. The basic optical and infrared properties of the 11 sources are presented in Table 1. The IRAC photometry is from the IRAC Shallow Survey (Eisenhardt et al. 2004).

3. OBSERVATIONS AND DATA REDUCTION

The spectroscopic observations were made with the IRS Short Low module in order 1 only (SL1) and with the Long Low module in orders 1 and 2 (LL1 and LL2), described in Houck et al. (2004). These orders give low-resolution spectral coverage from $\sim$8 to $\sim$35 μm. Sources were placed on the slits by offsetting from a nearby 2MASS star. The integration times for individual sources are given in Table 2.

Because these faint sources are dominated by background signal, we restrict the number of pixels used to define the source spectrum, applying an average extraction width of only 4 pixels (which scales with wavelength). This improves the signal-to-noise ratio (S/N), although some source flux in outlying pixels is lost so a correction is needed to change the fluxes obtained with the narrow extraction to the fluxes that would be measured with a standard extraction. This flux correction is derived empirically by extracting an unresolved source of high S/N with both techniques and is a correction of about 10%, although the correction varies with order and with wavelength.

The background that was subtracted for LL1 or LL2 includes co-added backgrounds from both nod positions having the source in the other slit (i.e., both nods on the LL1 slit when the source is in the LL2 slit), added together with the alternative nod position in the same slit, yielding a background observation with 3 times the integration time as for the source. For SL1, there was no separate background observation with the source in the SL2 slit, so background subtraction was done between co-added images of the two nod positions in SL1. Independent spectral extractions for each nod position were compared to reject highly outlying pixels in either spectrum, and a final mean spectrum was produced. Data were processed with version 13.0 of the SSC pipeline, and extraction of source spectra was done with the SMART analysis package (Higdon et al. 2004).

4. IRS SPECTRAL CHARACTERISTICS

The IRS spectra of the eleven 70 μm–selected sources are presented in Figure 1. They are boxcar-smoothed over a resolution element (approximately 2 pixels). Most of the sample (7 of 11) exhibit PAH emission features with measurable 6.2 μm PAH equivalent widths in their infrared spectra and are hereafter refered to as PAH-dominated sources (denoted as "sb" in Table 2). The large PAH equivalent widths are consistent with them being starburst-dominated sources and was anticipated because the large 70 μm fluxes imply that the spectra are dominated by dust that is cooler than that typically associated with AGNs. The remaining four sources exhibit strong 9.7 μm silicate absorption features, no obvious PAH emission features, and are classified as absorption-dominated sources (denoted as "abs" in Table 2).

For the PAH-dominated sources, redshifts are determined from the strong PAH emission features at rest wavelengths 6.2, 7.7, and 11.3 μm. With sufficient S/Ns, use of these features gives

TABLE 2
IRS Properties and Derived Physical Properties

IRS ID	Exposure Time[a] (s)	IRS z	$\nu L_\nu(6\ \mu\mathrm{m})$ [log(ergs s^{-1})]	$\nu L_\nu(7.7\ \mu\mathrm{m})$[b] [log(ergs s^{-1})]	$L_{\mathrm{IR}}(7.7)$[c] ($\log L_\odot$)	$L_{\mathrm{IR}}(24{+}70{+}160)$[d] ($\log L_\odot$)	SFR[e] ($M_\odot$ yr^{-1})	$f(15)/f(6)$	S_{10}[f]	PAH EW[g] (μm)	IRS Class[h]
70Bootes1	480,1200	0.501	43.89	44.53	11.72	12.15	90	4.2	...	0.26 ± 0.05	sb
70Bootes2	480,1200	0.366	43.65	44.18	11.36	11.79	40	1.8	...	0.85 ± 0.17	sb
70Bootes3	600,1440	0.986	44.69	45.37	12.56	13.05	625	4.3	...	0.48 ± 0.05	sb
70Bootes4	480,1200	0.975	44.24	45.32	12.51	12.95	565	9.6	...	0.59 ± 0.07	sb
70Bootes5	240,480	1.21	45.51	...	...	13.24	...	7.1	−1.0	<0.02	abs
70Bootes6	240,480	0.94	45.27	...	...	13.01	...	4.0	−1.9	<0.01	abs
70Bootes7	480,960	0.664	44.46	45.20	12.39	12.61	430	3.4	...	0.29 ± 0.04	sb
70Bootes8	240,480	0.81	44.79	...	...	12.88	...	7.7	−3.6	<0.03	abs
70Bootes9	240,480	0.668	44.62	45.43	12.62	12.81	720	4.0	...	0.53 ± 0.04	sb
70Bootes10	480,960	0.512	44.43	44.80	11.98	12.41	170	2.1	...	0.13 ± 0.01	sb
70Bootes11[i].....	240,480	0.48	44.75	...	...	12.49	...	8.3	−2.2	<0.02	abs

[a] Total integration times in SL1 (first entry) and each of LL1 and LL2 (second entry; same for each).
[b] 7.7 μm luminosity in source rest frame, determined from peak flux density of 7.7 μm feature without continuum subtraction.
[c] Infrared luminosity derived using the relation: $\log[L_{\mathrm{IR}}] = \log[\nu L_\nu(7.7\ \mu\mathrm{m})] + 0.78$ from Houck et al. (2007).
[d] Minimum infrared luminosity estimated from $L_{\mathrm{IR}} = [\nu L_\nu(24\ \mu\mathrm{m}) + \nu L_\nu(70\ \mu\mathrm{m}) + \nu L_\nu(160\ \mu\mathrm{m})] \times (1+z)$.
[e] Star formation rate derived from infrared luminosity using relation from Kennicutt (1998).
[f] Silicate absorption strength as defined in § 4.2.
[g] Rest-frame equivalent width of 6.2 μm PAH emission feature.
[h] PAH- and absorption-dominated sources are denoted "sb" and "abs," respectively. See § 4 for definitions of these terms.
[i] Object 8 in Houck et al. (2007).

redshifts consistent with optically derived redshifts to ±0.001 (Houck et al. 2005). Redshift precision for faint sources depends on the S/N, so for the spectra with PAH features, we consider the redshifts accurate only to ±0.05. For the absorbed sources, redshifts are determined primarily from the localized maximum in the IRS continuum, or "hump," which is blueward of the absorption feature. In the absorption-dominated sources, this feature is produced by absorption on either side of the feature, and with a possible contribution of 7.7 μm PAH emission in composite sources. We determine redshifts for absorption-dominated sources by assuming this hump has a rest-frame wavelength of 7.9 μm (see average spectra in Hao et al. 2007 and Spoon et al. 2007). Comparison with optical redshifts (e.g., Brand et al. 2007) suggests that they can be uncertain to ±0.1 in z.

We constructed an average mid-infrared spectra of the seven sources classified as PAH-dominated and for the four sources classified as absorption-dominated. This was achieved by wavelength correcting each individual spectrum to the rest frame ($z = 0$), interpolating them to a common wavelength scale of ≈0.1 μm pixel^{-1}, and taking a straight (nonweighted) average at each wavelength position. The resulting average spectra are shown in Figure 2. We discuss each class in turn.

4.1. *PAH-dominated* 70 μm *Sources*

The average IRS spectrum of the seven PAH-dominated sources in Figure 2 is characteristic of classical starbursts. The spectrum is very similar in shape to the average low-redshift (and lower luminosity) starburst template presented by Brandl et al. (2006), although the PAH emission features at 11.3 and 12.7 μm appear to be weaker in relation to the 7.7 μm PAH emission feature. The presence of low-ionization [Ne II] λ12.81 μm and [Ne III] λ15.56 μm emission lines and lack of significant high-ionization features such as [Ne V] λ14.32 μm are also very typical of starbursts. There is a possible detection of the rotational H_2 S(3) λ9.7 μm emission line in the averaged spectrum. This feature is seen in both high- and low-resolution IRS spectra of nearby starburst galaxies (e.g., Brandl et al. 2006; Higdon et al. 2006; Farrah et al. 2007; Armus et al. 2007) and suggests the presence of warm molecular gas. We measure the rest-frame 6.2 μm PAH equivalent widths by fitting a single Gaussian and using the continuum adjacent to the feature, between 5.5 and 7 μm. The values shown in Table 2 are similar to that of the lower redshift starburst galaxies presented by Brandl et al. (2006) and Desai et al. (2007).

These sources are interesting because of their extreme mid-infrared luminosities and red colors. The median continuum luminosity is $\nu L_\nu(6\ \mu\mathrm{m}) = 4 \times 10^{44}$ ergs s^{-1} ($1 \times 10^{11}\ L_\odot$). For comparison, the median luminosity for starbursts in the Boötes $f_{24} > 10$ mJy sample of Houck et al. (2007) is 1×10^{43} ergs s^{-1} ($3 \times 10^9\ L_\odot$) and for the prototype starburst NGC 7714 of Brandl et al. (2006) is 5×10^{42} ergs s^{-1} ($1 \times 10^9\ L_\odot$). In Figure 3 we compare the PAH luminosities, $\log[\nu L_\nu(7.7\ \mu\mathrm{m})]$, of our sample to other starbursts. The mean PAH luminosity of the PAH-dominated sources is orders of magnitude larger than that of the local starbursts from Brandl et al. (2006). The least luminous sources in our sample are comparable to the most luminous starbursts in the local universe. The luminosities are slightly lower than those of the high-redshift starbursts from Weedman et al. (2006a), which were chosen from the existence of a stellar photospheric peak in their near-IR SEDs. If we use the conversion in Houck et al. (2007) between the 7.7 μm PAH luminosity and star formation rate, we find that our most luminous source has a star formation rate of ∼720 $M_\odot$ yr^{-1}. This is only ∼50% lower than the upper limit on the Hα estimated star formation rates in local bright galaxies (Kennicutt 1998). Table 2 shows that these sources have larger infrared luminosities (as estimated from their 24, 70, and 160 μm luminosities) than those estimated from their 7.7 μm PAH luminosities. Their infrared luminosities are among the largest known for star-forming galaxies.

We measure the rest-frame $f_\nu(6\ \mu\mathrm{m})$ and $f_\nu(15\ \mu\mathrm{m})$ flux densities from the IRS spectra; $f_\nu(6\ \mu\mathrm{m})$ is measured just shortward of 6 μm to avoid the 6.2 μm PAH feature and provide a measurement of the hot dust continuum. In Figure 4 we show the distribution of 6 μm luminosities ($\nu L_{6\ \mu\mathrm{m}}$) as a function of continuum slope as measured by the rest-frame flux density ratio, $\nu f_\nu(15\ \mu\mathrm{m})/\nu f_\nu(6\ \mu\mathrm{m})$, and observed flux density ratio, $\nu f_\nu(70\ \mu\mathrm{m})/\nu f_\nu(24\ \mu\mathrm{m})$. The PAH-dominated sources have a lower mean $\nu f_\nu(15\ \mu\mathrm{m})/\nu f_\nu(6\ \mu\mathrm{m})$ than that of the lower

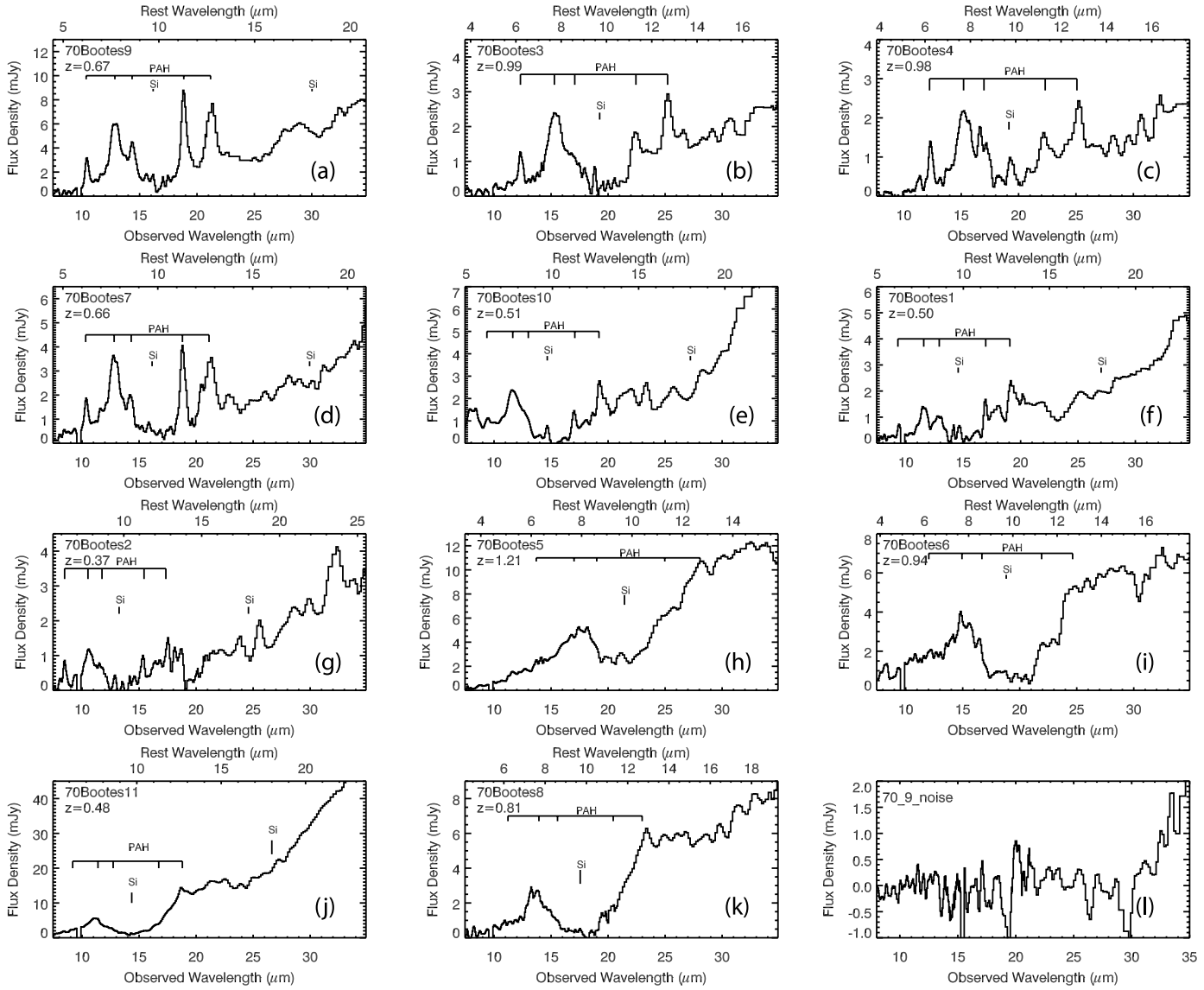

FIG. 1.—IRS spectra of 70 μm–selected luminous infrared galaxies. The sources are divided into (*a*–*g*) PAH-dominated and (*h*–*k*) absorption-dominated sources. The PAH-dominated sources are ordered by their 7.7 μm PAH luminosities (from strongest to weakest). The absorption-dominated sources are ordered by their silicate absorption strengths (shallow to deep). The spectra are boxcar-smoothed over a resolution element (approximately 2 pixels). The expected positions of the PAH emission features and silicate absorption features are shown. The measured equivalent widths of the PAH features and silicate absorption depths are given in Table 2. Also plotted is (*l*) a typical noise spectrum (for 70Bootes9).

luminosity starbursts of Brandl et al. (2006). Although this could suggest a contribution from an AGN to the infrared emission (since the hot dust results in a shallower spectral slope), a larger sample size is needed to show this with any confidence.

4.2. *Absorption-dominated* 70 μm *Sources*

The four absorption-dominated 70 μm sources have IRS spectra that are generally more characteristic of AGNs; they have no obvious PAH emission features (6.2 μm PAH equivalent width <0.03 μm) but deep silicate absorption features. They have 6 μm luminosities that are larger than those of the PAH-dominated sources and similar to those of the X-ray–selected AGNs in Brand et al. (2007). The infrared luminosities are also very large [$L_{\rm IR} \sim (0.3\text{–}1.7) \times 10^{13}\ L_{\odot}$].

We measure the silicate strength S_{10},

$$S_{10} = \ln \frac{f_{\rm obs}(10\ \mu{\rm m})}{f_{\rm cont}(10\ \mu{\rm m})}, \qquad (1)$$

using the method of Spoon et al. (2007), where $f_{\rm obs}(10\ \mu{\rm m})$ is the observed flux density at the peak of the 10 μm feature and $f_{\rm cont}(10\ \mu{\rm m})$ is the continuum flux at the peak wavelength, extrapolated from the continuum to either side. The silicate absorption depths are $S_{10} = -1.0, -1.9, -3.6$, and -2.2 for 70Bootes5, 70Bootes6, 70Bootes8, and 70Bootes11, respectively. These correspond to very heavy absorption, similar to the median for ULIRGs in Hao et al. (2007) and Spoon et al. (2007) ($S_{10} = -1.6$) and places them among the most heavily absorbed sources known (the most extreme example known has $S_{10} = -4.0$; Spoon et al. 2006). Hao et al. (2007) find that the silicate strength correlates with the infrared slope at high mid-IR wavelengths (14–30 μm) but not at lower mid-IR wavelengths (5–14 μm), supporting the idea that the silicate feature arises in the cooler dust [although note that no correlation between the $f_\nu(60\ \mu{\rm m})/f_\nu(25\ \mu{\rm m})$ flux density ratio and silicate strength is seen by Imanishi et al. 2007 in their sample of low-redshift ULIRGs]. Given that our selection criteria preferentially pick sources that are bright at 70 μm, the

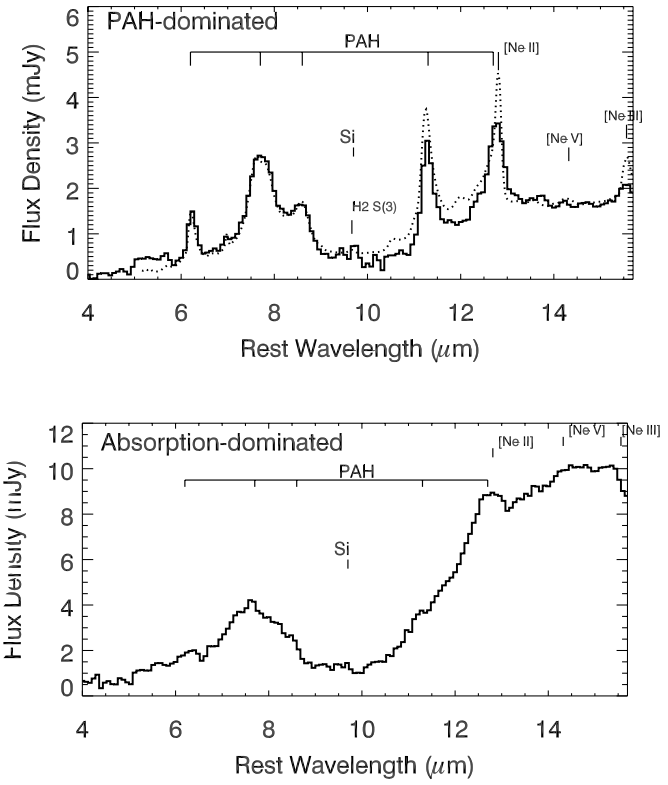

FIG. 2.—Average IRS spectrum of PAH-dominated sources (*top*) and absorption-dominated sources (*bottom*). The expected positions of typically strong emission lines and the silicate absorption line are plotted. The average IRS spectrum of low-redshift starburst galaxies from Brandl et al. (2006) is overplotted for the PAH-dominated spectrum (normalized to the 7.7 μm peak flux; *dotted line*).

large silicate strengths for the absorption-dominated sources are consistent with the findings of Hao et al. (2007).

Are these sources powered by AGNs or starburst activity? The individual spectra show no significant PAH-emission features (although there is a hint of the 7.7, 8.6, and 12.7 μm PAH features in the averaged spectrum in Fig. 2), so they appear most similar

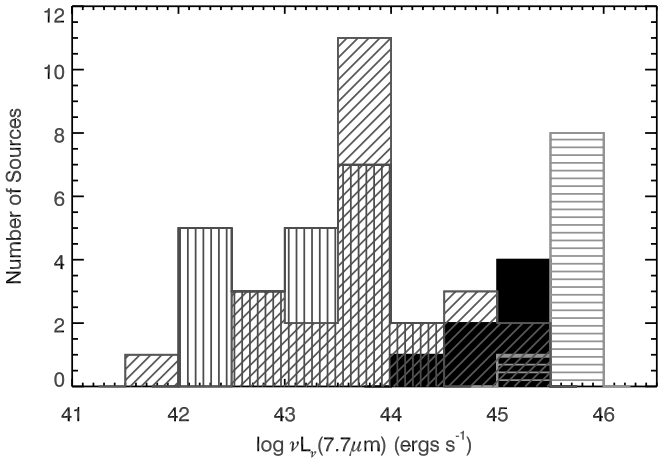

FIG. 3.—Histogram showing the 7.7 μm PAH luminosities, log[$\nu L\nu$(7.7 μm)], of the 70 μm PAH-dominated sources in our sample (*filled histogram*). For comparison, we show the local starbursts from Brandl et al. (2006; *vertical stripes*), the 10 mJy PAH-dominated sample from Houck et al. (2007; *diagonal stripes*), and the high-redshift starburst sample from Weedman et al. (2006a; *horizontal stripes*). [*See the electronic edition of the Journal for a color version of this figure.*]

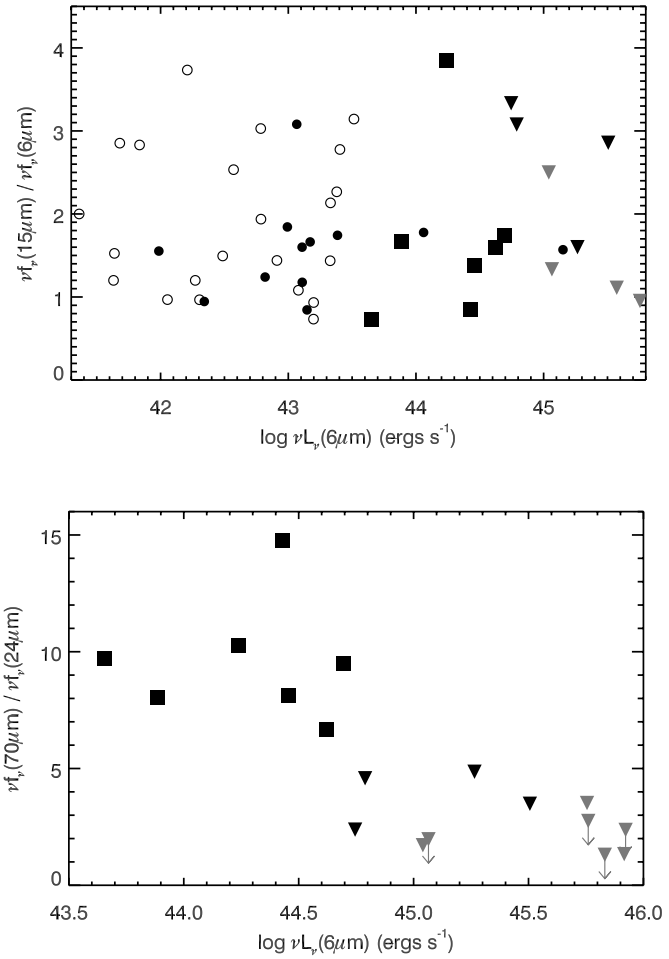

FIG. 4.—The log[νL_ν(6 μm)] as a function of rest-frame νf_ν(15 μm)/νf_ν(6 μm) ratio (*top*) and observed frame νf_ν(70 μm)/νf_ν(24 μm) ratio (*bottom*). PAH-dominated sources are represented by large black squares, absorption-dominated sources are represented by large black triangles, small filled circles represent PAH emission sources from the Boötes 10 mJy sample (Houck et al. 2007), small open circles represent local starbursts from Brandl et al. (2006), and large triangles represent X-ray–selected AGNs from Brand et al. (2007). [*See the electronic edition of the Journal for a color version of this figure.*]

to class 3A (little to no PAH emission, strong silicate absorption) in the scheme of Spoon et al. (2007). The IRS spectra are similar to those of two sources with deep silicate absorption strengths in a sample of 87 local Seyfert galaxies presented by Buchanan et al. (2006). Farrah et al. (2007) suggest that sources with very deep silicate absorption are likely to be AGN-dominated sources. The four sources have the largest 6 μm rest-frame luminosities in the sample and large infrared luminosities, again suggesting AGN activity. We observe no significant [Ne v] emission line that we might expect for AGN-dominated sources. However, given that [Ne v] often has a low equivalent width and that there are only four IRS spectra with low S/N at the observed wavelength of [Ne v] (see noise spectrum in Fig. 1), this is not strong evidence against a large contribution from AGN emission.

Because AGN-dominated galaxies typically have shallower mid-IR slopes than starburst-dominated galaxies (e.g., Brand et al. 2006), measuring flux density ratios at wavelengths free of strong absorption or emission lines may help in determining their primary power source. For heavily absorbed sources, estimating the slope at large rest-frame mid-infrared wavelengths is important because dust may absorb near-IR photons and re-emit them at longer wavelengths, steepening the spectral slope. Figure 4

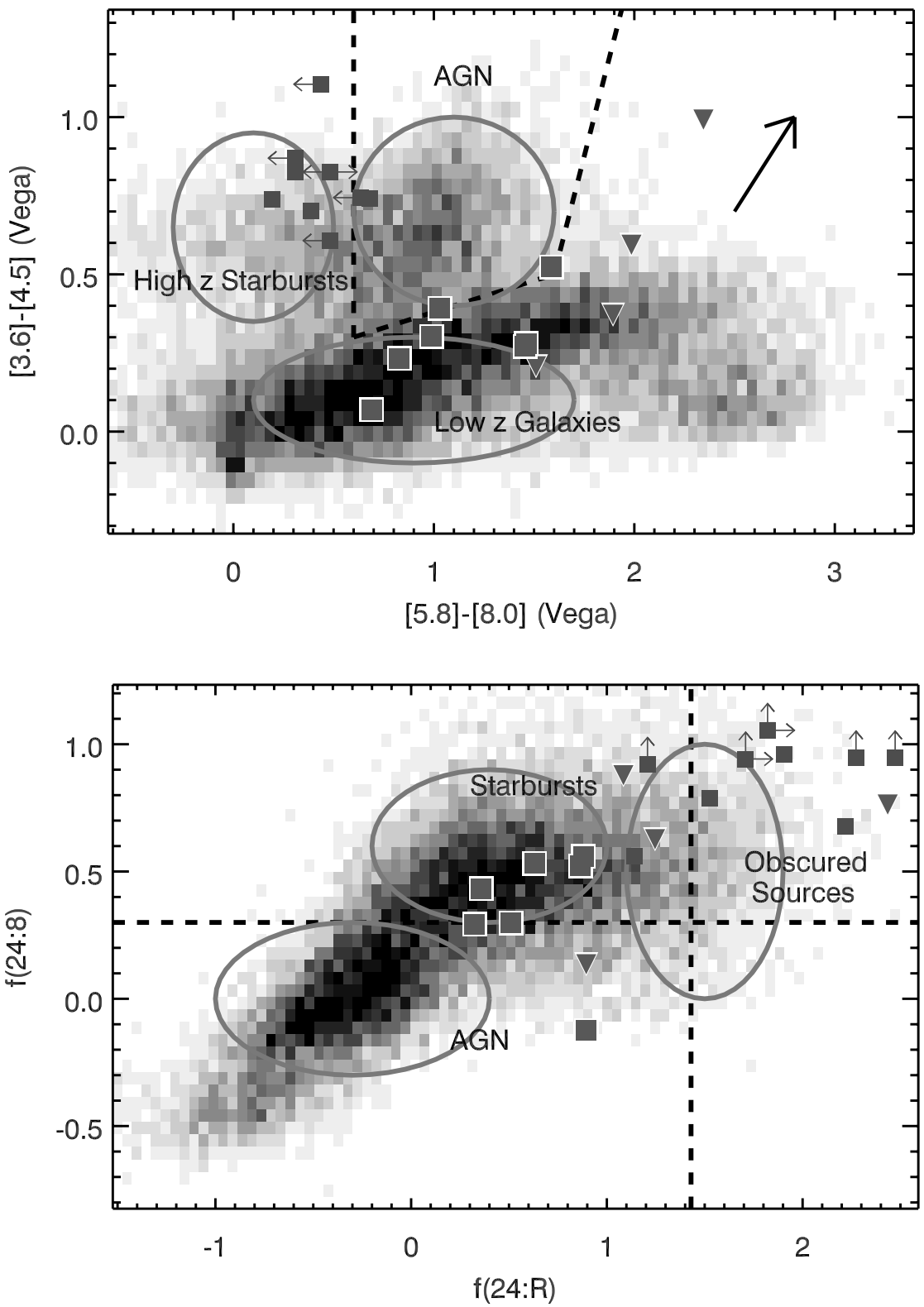

FIG. 5.—IRAC color-color diagram (*top*) and 24 to 8 μm vs. 24 to 0.7 μm color-color diagram (*bottom*) for 70 μm–selected IRS sources from Boötes (*large symbols*) and starburst-dominated sources from Weedman et al. (2006a; *smaller squares*). The Boötes sources are split into silicate absorption-dominated sources (*large triangles*) and PAH-dominated sources (*large squares*). We show the distribution of all ≈10,000 MIPS sources with $f_{24} > 0.5$ mJy in gray scale. The rough regions expected to be inhabited by different populations are also shown. The black dashed line in the top figure is that proposed by Stern et al. (2005) to empirically separate AGNs from Galactic stars and normal galaxies. The arrow shows the reddening curve estimated from the $R_V = 3.1$ dust model of Draine (2003) for a $z = 1$ source. In the bottom figure, the vertical dashed line shows the $R - [24] > 14[\log(\nu f_\nu(24)/\nu f_\nu(R)) > 1.43]$ criteria used to select the powerful obscured sources presented in Houck et al. (2005) and Weedman et al. (2006b), and the horizontal dashed line shows the 24 to 8 μm color criteria used by Brand et al. (2006) to roughly divide steeper spectrum starburst sources from shallow spectrum AGN-dominated sources at $z > 0.6$. [*See the electronic edition of the Journal for a color version of this figure.*]

shows that the absorption-dominated sources have observed-frame $\nu f_\nu(70\ \mu\text{m})/\nu f_\nu(24\ \mu\text{m})$ flux density ratios that are smaller than the PAH-dominated sources and closer to that of the X-ray–selected AGNs presented in Brand et al. (2007), suggesting that they have shallower infrared spectral slopes indicative of AGN-dominated sources. We note that one must be cautious in interpreting these results since the flux densities are in the observed frame and the rest-frame flux density ratio may vary with redshift. Although we can directly measure rest-frame flux density ratios at shorter wavelengths, these wavelengths are more likely to be affected by absorption. The $f_\nu(15\ \mu\text{m})/f_\nu(6\ \mu\text{m})$ flux density ratios of absorption-dominated sources are generally larger than those of the PAH-dominated sources. We suggest that strong dust absorption in the absorption-dominated sources results in a steeper infrared slope at these shorter infrared wavelengths, despite the fact that they have small $\nu f_\nu(70\ \mu\text{m})/\nu f_\nu(24\ \mu\text{m})$ flux density ratios and are likely to be dominated by AGNs.

We conclude that these are examples of very obscured sources, which are likely to be powered by AGNs. However, we cannot rule out the possibility of them being powered by deeply embedded starbursts. If the mid-IR emission of these sources is dominated by AGNs, this implies that ≈36% of sources selected to have luminous 70 μm emission are AGN-dominated. Perhaps the 70 μm emission, which traces cooler dust, is also powered largely by AGNs (see, e.g., Imanishi et al. 2007). In this cases, large 70 μm luminosities could be generated because the AGNs are so heavily absorbed by dust that a large fraction of the hot dust emission is absorbed and re-emitted at longer wavelengths. Alternatively, if a large fraction of the mid-IR emission originates from star formation activity, this implies that star formation activity as traced by mid-IR signatures can be hidden by obscuration and/or low-level AGN activity. Follow-up multiwavelength observations (optical spectroscopy, deep X-ray, and radio imaging) are clearly needed to fully determine the nature of these rare sources.

5. INFRARED AND INFRARED-TO-OPTICAL COLORS OF 70 μm SELECTED SOURCES

To help provide further insight as to the nature of the PAH- and absorption-dominated sources, we show the IRAC color-color diagram for our IRS sources in Figure 5*a*. For both the PAH-dominated and absorption-dominated sources, the colors are consistent with the expected positions of starburst-dominated, relatively low redshift galaxies (see also Yan et al. 2004; Sajina et al. 2005). Although we have concluded in previous sections that the absorption-dominated sources are probably largely powered by AGN emission, they do not fall into the "AGN wedge" of Stern et al. (2005). This is likely due to very heavy obscuration of the AGN. The IRAC colors of the absorption-dominated sources are consistent with their emission coming predominantly from heavily reddened star formation processes (see reddening arrow estimated from the $R_V = 3.1$ dust model of Draine 2003). The IRAC colors are redder than the PAH-dominated sources, consistent with them being more dusty and obscured than the PAH-dominated sources.

We also plot the IRAC colors of the starburst-dominated sources selected by Weedman et al. (2006a) to have optical and near-IR SEDs showing a luminosity peak from stellar photospheric emission at $1.0 < z < 1.9$. These sources have (by design) red [3.6]−[4.5] colors but blue [5.8]−[8.0] colors and confirm that sources in this region tend to be high-redshift, starburst-dominated sources. This region becomes more heavily populated at lower 24 μm fluxes, consistent with the population becoming more dominated by starbursts sources at fainter f_{24} as found by Brand et al. (2006).

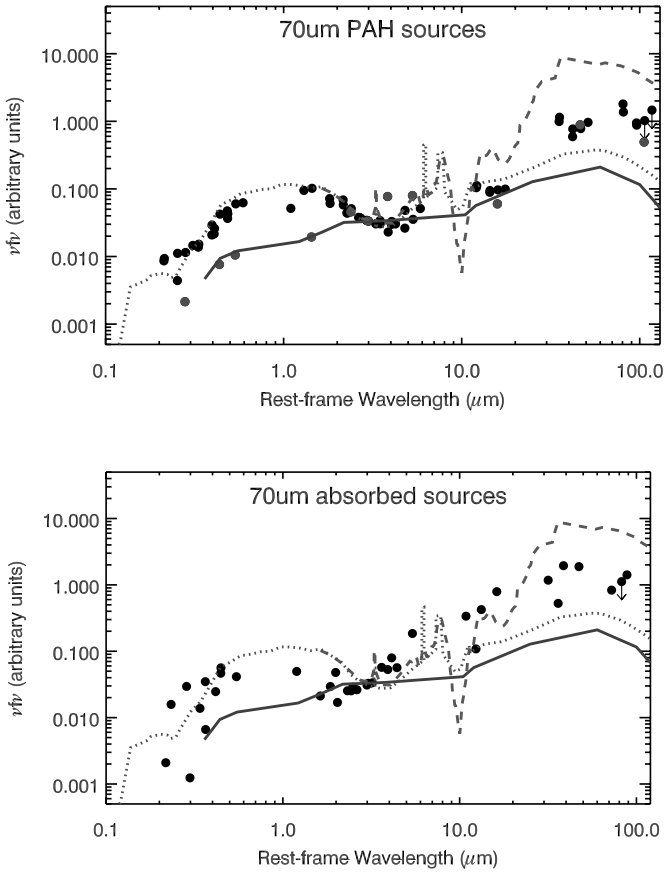

FIG. 6.—Optical to far-IR SEDs for PAH-dominated sources (*top*) and absorption-dominated sources (*bottom*). The individual spectra are scaled to have the same 3 μm flux density. Also plotted are SED templates of Mrk 231 (*solid line*), Arp 220 (*dashed line*; Silva et al. 1998), and M82 (*dotted line*; Silva et al. 1998). For the PAH-dominated spectra, most SEDs are similar to M82 below ~15 μm. 70Bootes10 is not well fit by M82, and its SED points are shown as light filled circles. [*See the electronic edition of the Journal for a color version of this figure.*]

To investigate the effects of obscuration, we show the 24 to 8 μm versus 24 to 0.7 μm color-color diagram for our sources in Figure 5*b* (see also Yan et al. 2004 for the location of different populations in this color-color space). The 24 to 0.7 μm color is a good indicator of obscuration, whereas the 24 to 8 μm color can be used as a crude measure of the spectral slope and hence the dust temperature distribution and whether the source is AGN- or starburst-dominated [Brand et al. 2006 find that AGN-dominated sources tend to have $f(24:8) < 0.3$ and starburst-dominated sources tend to have $f(24:8) > 0.3$; see also Yan et al. 2004]. The PAH-dominated, 70 μm–selected sources have lower $f(24:R)$ ratios than the absorption-dominated sources. Because PAH emission features can fall into the 8 μm IRAC wave band for $z < 0.6$, the 24 to 8 μm color is not a good indicator for most of these sources. The absorption-dominated 70 μm sources have higher $f(24:R)$ ratios than the PAH-dominated sources and steep spectral slopes, again consistent with them being more obscured. The starburst sources from Weedman et al. (2006a) have high $f(24:R$ ratios and $f(24:8)$ ratios consistent with them being higher redshift, obscured starburst-dominated sources.

6. MULTIWAVELENGTH SEDs

In Figure 6 we show the rest-frame multiwavelength (B_w, R, I, K, 3.6, 4.5, 5.8, 8, 24, 70, and 160 μm) SEDs for the PAH-dominated and absorption-dominated sources. We also show the SEDs of M82, Arp 220, and Mrk 231. M82 is the nearest

example of a starbursting galaxy and is often considered the prototype of the starburst phenomena (e.g., Rieke et al. 1980). Arp 220 is a starburst-dominated ULIRG with strong dust extinction (e.g., Soifer et al. 1984; Sturm et al. 1996). Mrk 231 is a local obscured AGN with a luminous circumnuclear starburst (e.g., Solomon et al. 1992; Weedman et al. 2005). The individual SEDs are normalized to the same flux density at 3 μm. All but one of the PAH-dominated sources are well fit by M82 blueward of 15 μm, consistent with them being starburst-dominated sources. 70Bootes10 (Fig. 6, *light filled circles*) is better fit by Mrk 231, suggesting that there is a large contribution of AGN emission in this source. 70Bootes10 is perhaps one of the most likely of the PAH-dominated sources to host an energetically important AGN, since it has the lowest 6.2 μm PAH equivalent width of all the PAH-dominated sources. The far-IR flux densities are between that of M82 and Arp 220, suggesting that the PAH-dominated sources have a large relative cool to hot dust content that is between these two local sources. The absorption-dominated sources have a larger variation in their SED shapes. None of the sources exhibit a strong near-IR "bump" that is characteristic of starburst galaxies. The far-IR slopes are steeper than those of Mrk 231, suggesting that these sources have a larger cool to hot dust ratio than Mrk 231. This may result from our selection criteria, which requires the galaxies to be very luminous at 70 μm.

7. CONCLUSIONS

We have presented *Spitzer* IRS mid-infrared spectra of a small sample of 11 sources from the *Spitzer* MIPS survey of the Boötes field using selection criteria based on 70 μm detections ($f_{70} > 30$ mJy) and faint optical magnitudes ($R > 20$). All the sources lie in the redshift range $0.3 < z < 1.3$, implying very large mid- and far-infrared luminosities. The IRS spectra of the 11 galaxies show either PAH emission features (7/11) or deep silicate absorption (4/11) features. The IRS spectra of the seven PAH-dominated sources are typical of classical starbursts, but with extremely large mid-infrared luminosities. This sample contains sources with very high PAH luminosities, implying star formation rates of up to 700 $M_{\odot}$ yr^{-1}. The PAH-dominated sources tend to have lower $\nu f_{\nu}(15\ \mu\mathrm{m})/\nu f_{\nu}(6\ \mu\mathrm{m})$ flux density ratios than that of lower redshift starburst galaxies with lower infrared luminosities. A larger sample is needed to show whether this is consistent with a contribution to the $f_{\nu}(6\ \mu\mathrm{m})$ luminosity from hot dust associated with an AGN in more luminous sources.

The four absorption-dominated sources have very deep silicate absorption features that are larger than the median of that of local ULIRGs, and their large $\nu f_{\nu}(15\ \mu\mathrm{m})/\nu f_{\nu}(6\ \mu\mathrm{m})$ flux density ratios suggest that their mid-infrared spectral slope is steep. This suggests that the energy source is embedded in large volumes of cool dust. The very red [5.8]−[8.0] and relatively red [3.6]−[4.5] colors also suggest a large amount of dust along the line of sight to these sources. The deep silicate absorption, small $\nu f_{\nu}(70\ \mu\mathrm{m})/\nu f_{\nu}(24\ \mu\mathrm{m})$ flux density ratio (which is less affected by dust obscuration than estimates from lower infrared wavelengths), and multiwavelength SEDs suggests that they are likely dominated by AGNs, although we cannot rule out that they are powered by very obscured starbursts. Follow-up multiwavelength observations such as optical spectroscopy and deep X-ray and radio observations may help to confirm their power source.

We thank our colleagues on the NDWFS, MIPS, IRS, AGES, and IRAC teams. K. B. is supported by the Giacconi fellowship at STScI. Support for this work by the IRS GTO team at Cornell University was provided by NASA through contract 1257184 issued by JPL/Caltech. This research is partially supported by the National Optical Astronomy Observatory, which is operated by the Association of Universities for Research in Astronomy (AURA), Inc., under a cooperative agreement with the National Science Foundation. This work is based on observations made with the *Spitzer Space Telescope*, which is operated by the Jet Propulsion Laboratory, California Institute of Technology, under a contract with NASA. The *Spitzer* MIPS and IRAC surveys of the Boötes region were obtained using GTO time provided by the *Spitzer* Infrared Spectrograph Team (PI: James Houck), M. Rieke, and the IRAC Team (PI: G. Fazio). IRAC is supported in part through contract 960541 issued by JPL. The IRS was a collaborative venture between Cornell University and Ball Aerospace Corporation funded by NASA through the Jet Propulsion Laboratory and the Ames Research Center.

REFERENCES

Armus, L., et al. 2007, ApJ, 656, 148
Brand, K., et al. 2007, ApJ, 663, 204
———. 2006, ApJ, 644, 143
Brandl, B. R., et al. 2006, ApJ, 653, 1129
Buchanan, C. L., Gallimore, J. F., O'Dea, C. P., Baum, S. A., Axon, D. J., Robinson, A., Elitzur, M., & Elvis, M. 2006, AJ, 132, 401
Desai, V., et al. 2007, ApJ, 669, 810
Draine, B. T. 2003, ARA&A, 41, 241
Eisenhardt, P. R., et al. 2004, ApJS, 154, 48
Elston, R. J., et al. 2006, ApJ, 639, 816
Farrah, D., et al. 2007, preprint (ArXiv:0706.0153)
Genzel, R., & Cesarsky, C. J. 2000, ARA&A, 38, 761
Hao, L., Weedman, D. W., Spoon, H. W. W., Marshall, J. A., Levenson, N. A., Elitzur, M., & Houck, J. R. 2007, ApJ, 655, L77
Higdon, S. J. U., Armus, L., Higdon, J. L., Soifer, B. T., & Spoon, H. W. W. 2006, ApJ, 648, 323
Higdon, S. J. U., et al. 2004, PASP, 116, 975
Houck, J. R., et al. 2004, ApJS, 154, 18
———. 2005, ApJ, 622, L105
———. 2007, ApJ, 671, 323
Imanishi, M., Dudley, C. C., Maiolino, R., Maloney, P. R., Nakagawa, T., & Risaliti, G. 2007, ApJS, 171, 72
Jannuzi, B. T., & Dey, A. 1999, in ASP Conf. Ser. 191: Photometric Redshifts and the Detection of High Redshift Galaxies, ed. R. Weymann, L. Storrie-Lombardi, M. Sawicki, & R. Brunner, (San Francisco: ASP), 111
Kennicutt, R. C., Jr. 1998, ARA&A, 36, 189
Le Floc'h, E., et al. 2005, ApJ, 632, 169
Lutz, D., Spoon, H. W. W., Rigopoulou, D., Moorwood, A. F. M., & Genzel, R. 1998, ApJ, 505, L103
Lutz, D., Yan, L., Armus, L., Helou, G., Tacconi, L. J., Genzel, R., & Baker, A. J. 2005, ApJ, 632, L13
Menéndez-Delmestre, K., et al. 2007, ApJ, 655, L65
Rieke, G. H., Lebofsky, M. J., Thompson, R. I., Low, F. J., & Tokunaga, A. T. 1980, ApJ, 238, 24
Rieke, G. H., et al. 2004, ApJS, 154, 25
Sajina, A., Lacy, M., & Scott, D. 2005, ApJ, 621, 256
Sajina, A., Yan, L., Armus, L., Choi, P., Fadda, D., Helou, G., & Spoon, H. 2007, ApJ, 664, 713
Sanders, D. B., Soifer, B. T., Elias, J. H., Madore, B. F., Matthews, K., Neugebauer, G., & Scoville, N. Z. 1988, ApJ, 325, 74
Saunders, W., Rowan-Robinson, M., Lawrence, A., Efstathiou, G., Kaiser, N., Ellis, R. S., & Frenk, C. S. 1990, MNRAS, 242, 318
Silva, L., Granato, G. L., Bressan, A., & Danese, L. 1998, ApJ, 509, 103
Smith, J. D. T., et al. 2007, ApJ, 656, 770
Soifer, B. T., Sanders, D. B., Madore, B. F., Neugebauer, G., Danielson, G. E., Elias, J. H., Lonsdale, C. J., & Rice, W. L. 1987, ApJ, 320, 238
Soifer, B. T., et al. 1984, ApJ, 283, L1
Solomon, P. M., Downes, D., & Radford, S. J. E. 1992, ApJ, 387, L55
Spoon, H. W. W., Marshall, J. A., Houck, J. R., Elitzur, M., Hao, L., Armus, L., Brandl, B. R., & Charmandaris, V. 2007, ApJ, 654, L49

Spoon, H. W. W., Tielens, A. G. G. M., Armus, L., Sloan, G. C., Sargent, B., Cami, J., Charmandaris, V., Houck, J. R., & Soifer, B. T. 2006, ApJ, 638, 759
Stern, D., et al. 2005, ApJ, 631, 163
Sturm, E., et al. 1996, A&A, 315, L133
Tran, Q. D., et al. 2001, ApJ, 552, 527
Weedman, D. W., et al. 2005, ApJ, 633, 706
Weedman, D. W., et al. 2006a, ApJ, 653, 101
———. 2006b, ApJ, 651, 101
Yan, L., et al. 2004, ApJS, 154, 60
———. 2005, ApJ, 628, 604
———. 2007, ApJ, 658, 778